Journal of Alloys and Compounds 898 (2022) 162974

Contents lists available at ScienceDirect

Journal of Alloys and Compounds

journal homepage: www.elsevier.com/locate/jalcom

Ag@SiO_2-embedded InGaN/GaN nanorod array white light-emitting diode with perovskite nanocrystal films

Do-Yeong Shin[a,1], Taehwan Kim[a,1], Ozgun Akyuz[b], Hilmi Volkan Demir[b,c], In-Hwan Lee[a,*]

[a] Department of Materials Science and Engineering, Korea University, Seoul 02841, Republic of Korea
[b] Department of Electrical and Electronics Engineering, Department of Physics, UNAM – Institute of Materials Science and Nanotechnology, Bilkent University, Ankara 06800, Turkey
[c] Luminous! Center of Excellence for Semiconductor Lighting and Displays, School of Electrical and Electronic Engineering, School of Physical and Materials Sciences, Nanyang Technological University, Singapore 639798, Singapore

ARTICLE INFO

Article history:
Received 20 October 2021
Received in revised form 23 November 2021
Accepted 25 November 2021
Available online 28 November 2021

Keywords:
White light-emitting diodes
Perovskite nanocrystals
Nanorod light-emitting diodes
Localized surface plasmon

ABSTRACT

White light-emitting diodes (LEDs) are great candidates for general lighting. Phosphors have commonly been used for the color conversion layers of white LEDs; however, they backscatter more than half of the down-converted light, which is lost within the device, thus degrading the overall performance. In this study, we propose and demonstrate white LEDs with improved efficiency enabled by the intimate integration of Ag@SiO_2-supported blue InGaN/GaN nanorod LEDs together with green- and red-emitting perovskite nanocrystal (PNC) films as color conversion layers. The photoluminescence (PL) intensity of the blue LEDs (BLEDs) was significantly enhanced owing to the localized surface plasmon (LSP) effect of Ag@SiO_2 nanoparticles. In addition, the perovskite PL intensity was improved by the high-power BLED backlight. The resulting PL intensity of the Ag@SiO_2 nanoparticle-embedded nanorod white LED was 62% greater than that of a planar white LED.

1. Introduction

High-efficiency white light-emitting diodes (LEDs) have been developed for solid-state lighting (SSL). The advantages of SSL include the high luminous efficiency, energy saving, small volume, and long persistence [1,2]. The phosphor-converted (pc) white LED is the most common type in SSL. The first example of pc-LEDs contained cerium-doped yttrium aluminum garnet (YAG:Ce) phosphor integrated with a gallium nitride (GaN)-based blue LED (BLED) [3]. However, the low light conversion efficiency and low color rendering index (CRI) due to weak red emission have been the common problems of using YAG:Ce^{3+} [4,5]. In addition, a part of the blue light (at a peak wavelength of approximately 450 nm) emitted by GaN LEDs is down-converted by the phosphor to produce yellow light (at a peak wavelength of approximately 545 nm); their combination results in white light generation. The major challenges regarding such pc-LEDs are achieving high chromatic stability, high luminous efficiency, and brilliant color rendering properties, all of which depend on the phosphor properties and efficiency of BLEDs.

As an alternative to YAG:Ce^{3+}, perovskites can generate more brilliant white light [6,7]. All-inorganic lead halide perovskite ($CsPbX_3$) nanocrystals (PNCs) offer outstanding optoelectronic properties including tunable emission, high photoluminescence quantum yields (PLQY), and narrow line-width emission across the whole visible spectrum depending on the nanocrystal size and halide ion composition [8–10]. As a result, PNCs are widely investigated for use in modern optoelectronic devices including solar cells, LEDs, photodetectors, and lasers [6,11–13]. However, several problems must be addressed for the widespread use of PNCs in practice. The most urgent problem is the long-term stability of PNCs under humid conditions [14]. This can be mitigated via passivation, e. g., with polydimethylsiloxane (PDMS) for long-term stability [15]. PNCs can be excited by UV or BLED backlight to obtain a wide color gamut with high light efficiency.

Furthermore, for high-efficiency white LEDs, the power of the backlighting BLED can be increased by improving the internal quantum efficiency (IQE), external quantum efficiency (EQE), and light extraction efficiency (LEE) to promote photon extraction [16]. Owing to their outstanding advantages, nanostructures are used in

* Corresponding author.
E-mail address: ihlee@korea.ac.kr (I.-H. Lee).
[1] Shin and Kim equally contribute to this work.

https://doi.org/10.1016/j.jallcom.2021.162974
0925-8388/

many devices such as super-bright LEDs, full color displays, and flexible LEDs [17,18]. For InGaN/GaN multiple quantum well (MQW)-based LEDs, nanorod (NR) structures can relieve strain and, thus, compensate for large lattice mismatch at heterointerfaces, which can enhance the radiative recombination efficiency and therefore the IQE of LED devices [19]. In addition, owing to the large sidewall surface of NRs, the LEE can be improved [18]. Previous studies reported the localized surface plasmon (LSP) effect using Ag@SiO_2 nanoparticles (NPs) [20]. If the LSP layer is sufficiently close (but not too close) to the MQW active layer of an LED and the MQW emission wavelength matches the LSP resonance energy, the LED performance can be boosted through the energy coupling (EC) mechanism from excitons in the active region of the LED to the LSP modes of the metal nanostructures.

In this study, the performance characteristics of white LEDs with high efficiency BLEDs as backlighting unit and PNC films as color conversion layers were studied. When the distance between PNCs is within several nanometers, Förster resonance energy transfer (FRET) occurs from green PNCs (with a large bandgap) to red PNCs (with a small bandgap) [21]. Because FRET is a non-radiative process, it should be suppressed for efficient down-conversion of lights. As PNC–polymer composites contain many PNCs with different bandgaps, FRET can occur in these samples [22]. In a polymer matrix that contains green and red emitting PNCs, the energy transfer from green to red PNCs causes the PL spectrum to be strongly weighted toward the red band. Researchers have reported that FRET can be mitigated in PNC–polymer composites by constructing bilayer film structures that emit in different colors separately [23]. In addition, red and green PNCs were separately mixed in polymer matrices and combined to prevent FRET by avoiding their aggregation [22].

2. Experimental

2.1. Fabrication of blue emitting InGaN/GaN NR arrays

An InGaN/GaN MQW epitaxial structure was grown via metal organic chemical vapor deposition to prepare Ga, In, and N precursors. The c-plane sapphire substrate was thermally annealed at 1100 °C for 10 min. Subsequently, a low-temperature GaN buffer layer was deposited on the sample. A 2 μm thick undoped GaN layer and a 10 μm thick n-type GaN layer were grown at 1060 °C. In the next step, five pairs of InGaN/GaN MQWs were grown on high-quality GaN epitaxial layers. The GaN barriers and InGaN wells were grown at 850 and 750 °C, respectively. Furthermore, a 300 nm thick p-type GaN layer was grown on top.

To prepare the NR LEDs, 1 μm thick SiO_2 and 80 nm thick Cr were deposited as a hardmask on the surface via plasma-enhanced chemical vapor deposition and e-beam evaporator, respectively. A monolayer of patterned PS nanospheres (diameter: 1 μm) was spin-coated onto the Cr/SiO_2/GaN substrate. The PS nanospheres were reduced in an O_2 plasma ashing process. In the next step, Cl_2/Ar-based reactive ion etching (RIE) was performed to transfer the pattern to the underlying Cr layer. The nanodot mask was transferred to the SiO_2 layer via CF_4-based RIE on the SiO_2/GaN substrate. With the prepared SiO_2 NR array as the etching mask, patterned InGaN/GaN NR structures could be fabricated on the sapphire substrate through inductively coupled plasma (ICP) etching with a Cl_2/BCl_3 gas mixture. In general, GaN NR arrays fabricated with the top-down method exhibit surface defects on the NR sidewalls owing to high-energy ion bombardment during plasma etching [17,24]. To retain the performance characteristics of the etched GaN NR LEDs, a KOH-based wet etching process (3 mol/L) was performed for 30 min [25]. The remainder of the SiO_2 NR arrays were removed by dipping the sample into a buffered oxide etchant. Consequently, cylindrical InGaN/GaN NR arrays remained on the sapphire substrate [26].

2.2. Synthesis of Ag@SiO_2

To synthesize SiO_2-capped Ag NPs, NH_4OH (28–30%), tetraethylorthosilicate (TEOS), and the prepared silver NPs were used. In addition, de-ionized (DI) water and ethanol were used in all processes [27]. The typical synthesis procedure is as follows: a 500 mL beaker was filled with 80 mL ethanol, 19 mL DI water, and 1 mL Ag NPs under vigorous magnetic stirring. After 10 min, 5 mL NH_4OH (28–30%) was added as a catalyst; subsequently, 40 μL pure TEOS was added to prepare the shell. The solution was stirred for another hour at room temperature. To remove residues and impurities, the synthesized Ag@SiO_2 NPs were centrifuged in ethanol at 7000 rpm for 20 min. The purified Ag@SiO_2 NPs were dispersed in 1 mL ethanol.

2.3. Fabrication of high-efficiency NR BLED

To coat the InGaN/GaN NR BLED with Ag@SiO_2, the latter was dispersed in 1 mL ethanol and 1 g PDMS (base and curing agent with a 10:1 wt mixing ratio), which had been uniformly mixed. The as-obtained mixed solution was degassed to remove completely bubbles in the Ag@SiO_2–PDMS mixture. In the next step, the mixture was spin-coated onto the NR BLED substrate. An Ag@SiO_2 film was obtained after curing the sample at 130 °C. Finally, the Ag@SiO_2 NPs on the top of the InGaN/GaN NRs were removed in an O_2/CH_4-based RIE process to prevent them from disturbing the incident laser beam and to facilitate the extraction of emitted light.

2.4. Synthesis method for PNCs

Green $CsPbBr_3$ NCs were synthesized with the method of Protesescu et al. [10]. First, to prepare the Cs precursor, 0.2 g Cs_2CO_3 was mixed in 10 mL 1-octadecence and 1 mL oleic acid (OA) at 150 °C for 10 min. For the $PbBr_2$ precursor, 0.07 g $PbBr_2$ was dissolved in 5 mL ODE, 0.5 mL OA, and 0.5 mL oleylamine at 180 °C for 10 min. The $PbBr_2$ precursor was rapidly added to 0.4 mL Cs precursor and cooled in an ice water bath for 1 min [28]. After the reactions had terminated, the synthesized PNCs were separated at 10,000 rpm for 20 min and re-dispersed in 1 mL toluene for further use. The red $CsPbI_3$ NCs were synthesized with the method of Ramasamy et al. [12]. The exchange reaction was performed by adding calculated amounts of ethanol solution of LiI to the $CsPbBr_3$ NCs in toluene at room temperature. This mixture was shaken vigorously, which changed the color from green to red. The reaction terminated within less than 5 s

2.5. Fabrication of white LED

To prepare a highly efficient pe-white LED, the prepared high-efficiency Ag@SiO_2-supported NR BLED substrates were coated with two different PNCs (green- and red-emitting PNCs), respectively. Each PNC type and 1 g PDMS (base and curing agent with 10:1 wt ratio) were added into a Teflon beaker and mixed to obtain a uniform mixture. The mixed solution was degassed to remove completely bubbles in the PNC–PDMS mixture. Finally, a PNC–PDMS color conversion film was obtained after curing the sample at 100 °C. To prepare the double layered PNC–PDMS film, a red-emitting layer and a green-emitting layer were sequentially spin-coated onto the sample.

3. Results and discussion

3.1. Characterizations

To record XRD patterns of the samples, we used a Rigaku SmartLab diffractometer with Cu Kα radiation (λ = 0.1546 nm) and a

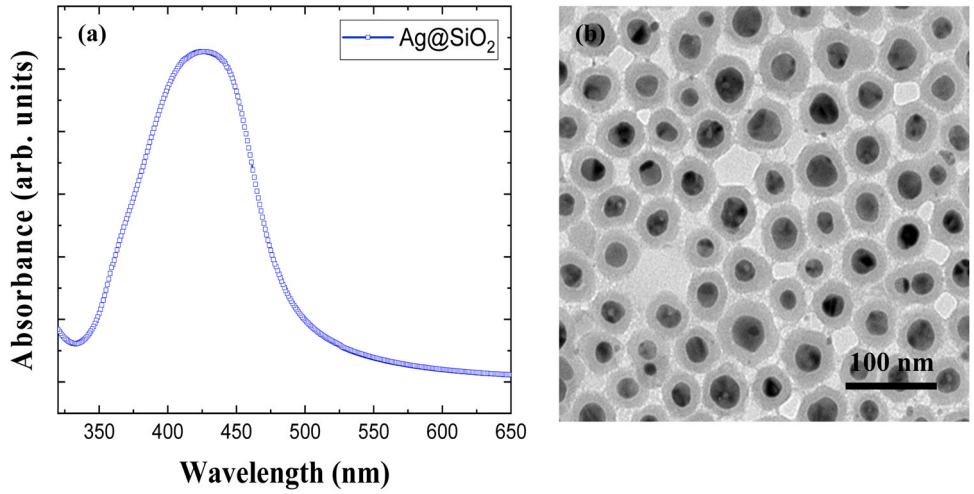

Fig. 1. (a) Absorbance spectrum and (b) TEM image of $Ag@SiO_2$ NPs synthesized with sol–gel method.

nickel filter. The PNC structures were analyzed with XPS (AXIS Ultra DLD, Kratos. Inc; monochromatic Al Kα radiation: 1486.6 eV, 150 W). The morphology was examined with field-emission SEM (SUPRA-40VP) and high-resolution TEM (JEOL-2010). The UV–vis spectra were recorded with a UV–vis spectrophotometer (UV-2550, Shimadzu). For the room-temperature PL measurements, a 405 nm laser with a 100 mm diameter and 25 mW power was used as the excitation source. The TRPL measurement was performed while exciting the LEDs under pulse excitation (pulse width: approximately 5 ns; center wavelength: approximately 405 nm); the measurement was recorded with a monochromator, photomultiplier tube, high-speed photodetector, and controller electronics. The optical properties of the pe-white light, including the CCT, CRI, and CIE coordinates were calculated with the method shown in our previously published paper [29]. All measurements were performed at room temperature.

3.2. Materials and device performance

The LSP resonance results of the NPs demonstrate that the fluorescence characteristics of samples with NPs are greatly affected by the $Ag@SiO_2$ layer of the light-emitting layer [19]. The distance from the metal surface is the most important factor for high EC efficiency. The minimum interspacing between the active layer and LSP of the metal NPs allows us to assume that the $Ag@SiO_2$ NPs are optimal for a stable and reliable improvement of the LED performance characteristics because they result in efficient EC between the LED active regions and NP-related LSPs. Based on this consideration, we embedded synthesized $Ag@SiO_2$ NPs in the NR LED. Fig. 1b shows a transmission electron microscopy (TEM) scan of the morphology of the $Ag@SiO_2$ NPs. They are mostly spherical; moreover, the Ag NPs are completely covered by a SiO_2 shell with approximately uniform thickness. The estimated size of the $Ag@SiO_2$ NPs ranges between 50 and 80 nm, and the SiO_2 shell is 20 nm thick. The UV–vis spectrum in Fig. 1a shows the $Ag@SiO_2$ NPs have an absorbance peak at 425 nm. The absorbance wavelength of these NPs is in the blue emission range of the NR LEDs; therefore, these NPs can be suitable for promoting EC via LSP mechanism [30,31].

Fig. 2 shows the morphologies, crystal structures, and optical properties of the as-synthesized $CsPbBr_3$ and $CsPbI_3$ NCs. The TEM images (Fig. 2(a and b)) were recorded to study the morphology of the as-prepared PNCs. The $CsPbBr_3$ NCs have cubic structures similar to those reported in the previous report on the low-temperature synthesis. Implication of ethanol-based lithium iodide (LiI) concentration promoted growth of the cubic structure. The TEM images reveal that the $CsPbBr_3$ and $CsPbI_3$ NCs have retained their cubic morphologies; however, they have different thicknesses. The $CsPbI_3$ NCs are thicker than the original $CsPbBr_3$ NCs. As shown in the X-ray diffractometer (XRD) data in Fig. 2c, the (200) reflection peak at 30.92° has shifted to a lower angle (29.31°) owing to lattice expansion caused by the substitution of larger I- ions for smaller Br- ions. In addition, the intensity of the XRD peaks has changed. For the iodide-exchanged samples, the intensity of the (200) peak is higher than those of the other planes. Thus, the $CsPbI_3$ NCs have grown along the (200) plane after the iodide exchange reaction. To investigate the surface composition and chemical states of the elements present in the $CsPbBr_3$ and $CsPbI_3$ thin films, X-ray photoelectron spectroscopy (XPS) measurements were performed. Fig. 2(d and e) display the complete XPS spectra of the samples with C, Cs, Pb, Br, and I signals.

Fig. 3 presents the absorbance and spectra of the $CsPbBr_3$ and $CsPbI_3$ NCs, which undergo halide exchange reactions at different LiI concentrations. The as-synthesized $CsPbBr_3$ NCs have an absorbance peak at approximately 505 nm, which experiences a redshift to 630 nm after the reaction with 60 µL 1 M LiI. With increasing LiI concentration, the absorbance peak experiences a redshift, which agrees well with the XRD measurements. Moreover, the (200) peak shifts toward lower angles, which indicates the substitution of Br^- with I^-. As shown in Fig. 3, the PL peak can shift from 520 to 630 nm with different LiI concentrations. The $CsPbBr_3$ and $CsPbI_3$ NCs exhibit strong absorbance and narrow luminescence peaks (full-width-at-half-maximum – FWHM = 23 and 31 nm, respectively).

Fig. 4 shows the 3-D sample structures and scanning electron microscopy (SEM) images of the NR LED, $Ag@SiO_2$ NP-embedded NR LED, and white LED with $Ag@SiO_2$ NP-embedded NRs and PNCs. Fig. 4(a and d) clearly show that the NRs have diameters of approximately 700–800 nm and lengths of approximately 3 µm. The distance between the NRs is approximately 300 nm. To study the EC mechanism between the NPs and NR LED, the synthesized $Ag@SiO_2$ NPs and PDMS were spin-coated onto the NR LEDs as shown in Fig. 4(b and e). As seen in Fig. 4e, the NPs on top of the NRs were clearly removed after ashing process to facilitate the extraction of emitted light, and the embedded NPs were close to the active layer of the NR LEDs. The preparation of the $Ag@SiO_2$-embedded NR BLED was presented in detail in our previous publication [20]. Owing to the tunable PL emission range that covers the entire visible wavelength range, the narrow FWHM, and high PLQY, PNCs have huge potential for color conversion layers in white LEDs that generate white light with a high color quality. Hence, as presented in Fig. 4(c and f), a prototype white LED with a neutral white light was

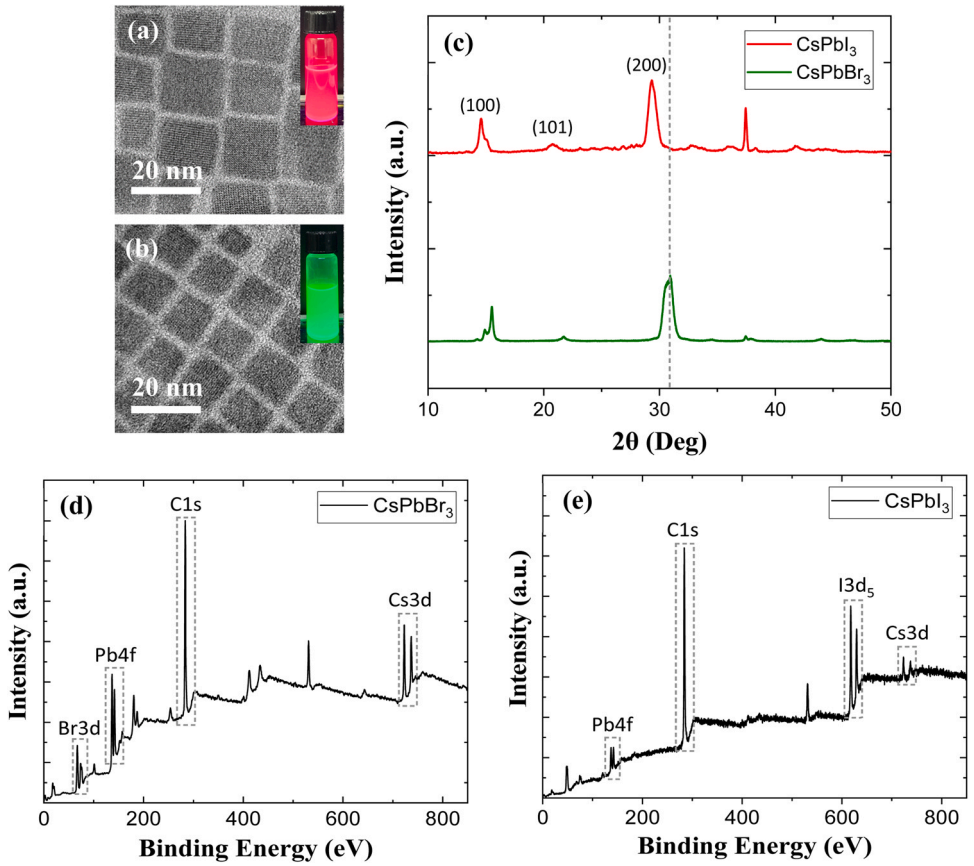

Fig. 2. TEM images of (a) $CsPbBr_3$ NCs and (b) $CsPbI_3$ NCs. (c) XRD patterns of $CsPbBr_3$ NCs (bottom, green) and $CsPbI_3$ (top, red). XPS full-range spectra of (d) $CsPbBr_3$ NCs (green) and (e) $CsPbI_3$ NCs (red).

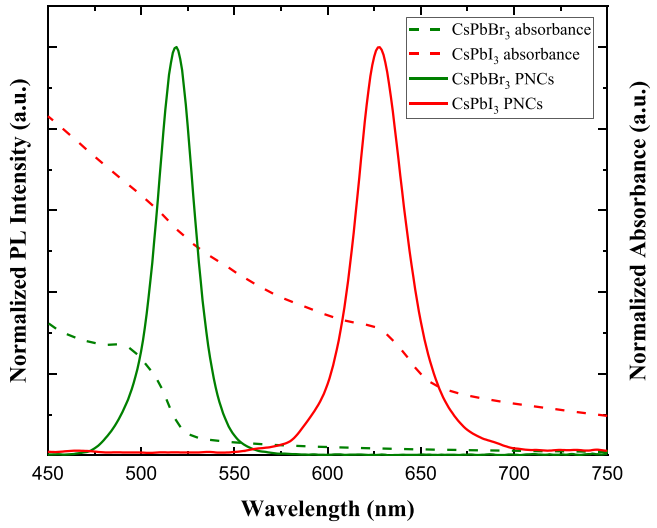

Fig. 3. Normalized PL intensity and absorbance of $CsPbBr_3$ NCs (green) and $CsPbI_3$ NCs (red).

prepared with thin layers containing PDMS-based perovskite NCs (green and red) in conjunction with an $Ag@SiO_2$-embedded NR BLED chip (λ_{peak}: approximately 455 nm). To prepare a highly efficient white LED, we adopted the $Ag@SiO_2$-embedded NR BLED as backlight unit. To avoid that the reabsorption and FRET cause a significant redshift of the desired final color of the white LED, we prepared a double-layer structure that comprises separated green and red emitting composite layers. First, the red emitting thin layer ($CsPbI_3$–PDMS) was deposited onto the $Ag@SiO_2$-embedded NR BLED; subsequently, the green emitting thin layer ($CsPbBr_3$–PDMS) was deposited onto the sample.

Fig. 5 compares the performance results of the as-grown planar LED, NR structure, and $Ag@SiO_2$ NP-embedded NR structure. The PL measurements were performed with near normal incidence (Fig. 5a). The PL peak wavelength of the planar sample (467 nm) experiences a blue-shift after the fabrication of NRs. This blueshift can be attributed to strain relaxation in the area of the etched sidewall [32,33]. The improved PL intensity is understood as follows: strain relaxation restores the tilted band to a flat band by increasing the overlap between the electron and hole wave functions; this increases the light oscillation strength and radiative recombination rate [19]. The luminescence peak occurs at 457 nm, and the PL intensity is 31% greater than that of the planar LED. The PL intensity of the $Ag@SiO_2$ embedded sample was increased owing to the LSP effect between the $Ag@SiO_2$ and the MQWs. Moreover, the efficiency is 45% greater than that of the planar LED and 11% greater than that of the NR LEDs. To understand the underlying mechanism behind these intensity improvements, the EC process of the NP-embedded NRs must be investigated. Usually, EC to non-radiative recombination in the emitter is limited to the distance of several tens of nanometers. In the case of the $Ag@SiO_2$ NPs, the Ag spheres are covered by a 20 nm SiO_2 shell. The SiO_2 shell provides a long enough separation, which prevents the tunneling of electrons. This suggests that $Ag@SiO_2$ NPs can prevent the energy loss of LSPs, thereby improving luminescence efficiency [34–36]. To present the LSP effect, Fig. 5b shows time-resolved photoluminescence (TRPL) spectra of NR LED and $Ag@SiO_2$-embedded NR LED. Both relaxation curves show initial fast decay regions, which is typical for InGaN/GaN MQWs. The fast decay is often believed to be due to excitonic relaxation and nonradiative relaxation. The measured effective lifetimes at 455 nm of the

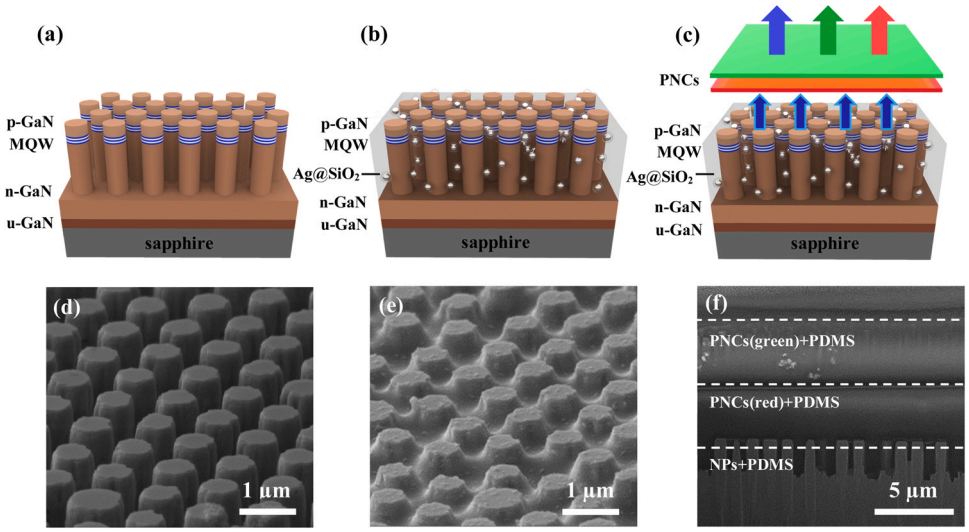

Fig. 4. Schematic structures of (a) NRs, (b) Ag@SiO_2-embedded NRs and (c) fabrication of white LED with PNC films. SEM images of (d) NR structures, (e) Ag@SiO_2-embedded NRs, and (f) PNC coating on Ag@SiO_2-embedded NR structure (f).

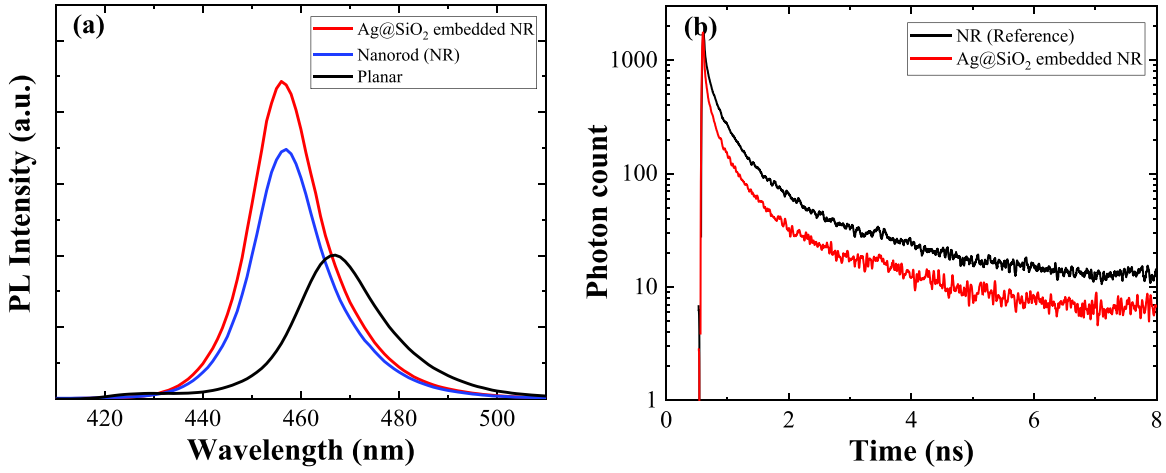

Fig. 5. (a) Room temperature PL spectra of planar, NR, and Ag@SiO_2 NP-embedded NR samples. (b) TRPL decay curves of reference NR LED and NP-embedded NR LED.

Table 1
Summarized PL enhancement and EC efficiency of the blue and white LEDs.

Structure		Peak wavelength(λ_{max}, nm)	FWHM(nm)	PL enhancement	EC efficiency
Blue LED	Planar	467	20.27	1	–
	NR	457	16.74	1.31	1
	Ag@SiO_2-embedded NR	457	16.65	1.45	1.57
White LED	Planar+PNCs	–	–	1	–
	NR+PNCs	–	–	1.10	–
	Ag@SiO_2-embedded NR+PNCs	–	–	1.62	–

reference NR and Ag@SiO_2-embedded NR LEDs are 3.41 and 2.48 ns, respectively. This results from the coupling of MQW excitation energy to the fast LSP channel from which the energy is converted into outside light [37]. From these transient PL results, the EC efficiency of each sample was calculated with the following equation: $\eta_{EC} = \tau_{LSP}^{-1}/(\tau_{LSP}^{-1} + \tau_{nanorod}^{-1})$; $\tau_{nanorod}$ (3.41 ns) and τ_{LSP} (2.48 ns) represent the decay times of the reference NR LED and NP-embedded NR LED, respectively. The calculated EC efficiency of Ag@SiO_2 LSP is 57%. Thus, the near-surface MQWs of the NRs close to NPs should be strongly affected by the LSP fringe field and recombination rates. In addition, the effective PL lifetime should be the sum of the reciprocal bulk and near-surface recombination lifetimes. These considerations suggest that the PL intensity increase and lifetime acceleration due to MQW-LSP coupling should be much higher than those calculated by the simple estimates above [38]. The PL enhancement and EC efficiency of the blue and white LEDs are summarized in Table 1.

Fig. 6 shows the performance results of the white LED. Based on this device structure, we investigated the photometric properties of the generated white light such as the correlated color temperature (CCT), color rendering index (CRI), and commission internationale de l'Eclairage (CIE) coordinates. In addition, to prove the improved PL efficiency, we compared the characteristics of the planer white LED, NR white LED, and Ag@SiO_2-embedded NR LED. The PL intensity of the Ag@SiO_2-embedded NR sample is 47% higher than that of the NR

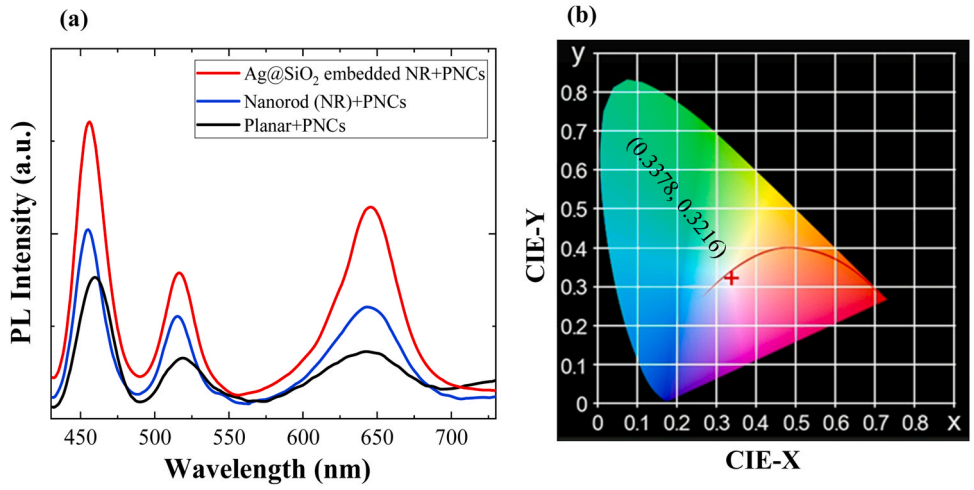

Fig. 6. (a) PL spectra of the fabricated pe-WLED with different BLED intensity. (b) CIE coordinates of the corresponding white light emission with Ag@SiO_2 embedded nanorod structure.

sample and 62% higher than that of the planar sample (see Fig. 6a). The white light from the Ag@SiO_2-embedded NR has resulted in a CRI of 87.7 with a CCT of 5975 K; thus, the sample provides a high-CRI white light. The inset in Fig. 6b shows the CIE diagram; (x, y) coordinates (0.3378, 0.3216) of the sample are very close to those of standard neutral white light (0.333, 0.333). Therefore, perovskite white (pe-white) LEDs with Ag@SiO_2-embedded NR BLEDs are promising candidates with improved efficiency and high color purity.

4. Conclusions

In conclusion, we have demonstrated a reliable approach to the fabrication of high-performance perovskite white LED. The presented color conversion layers with PNCs ($CsPbX_3$) and PDMS mixture can generate high PLQY and high CRI performance. In addition, use of Ag@SiO_2-embedded InGaN/GaN NR structure to replace planar BLED provides an effective way of improving the BLED efficiency, resulting in highly efficient pe-white LED. Consequently, the pe-white LED has a CRI of 87.7, CCT of 5975 K, and white CIE coordinates of (0.3378, 0.3216). The fabricated white LED with the highly efficient BLED structure opens up new possibilities for optoelectronic applications.

CRediT authorship contribution statement

Do-Yeong Shin: Conceptualization, Methodology, Formal analysis, Investigation, Resources, Data curation, Writing – original draft. **Taehwan Kim:** Conceptualization, Data curation, Formal analysis, Investigation, Resources. **Ozgun Akyuz:** Writing – review & editing, Visualization, Supervision. **Hilmi Volkan Demir:** Writing – review & editing, Funding acquisition. **In-Hwan Lee:** Writing – review & editing, Visualization, Supervision, Project administration, Funding acquisition.

Declaration of Competing Interest

The authors declare that they have no known competing financial interests or personal relationships that could have appeared to influence the work reported in this paper.

Acknowledgement

This research study was supported by the National Research Foundation of Korea (NRF) grant funded by the Korean Government (MSIT) (NRF-2019K1A3A1A39103053) and by the Scientific and Technological Research Council of Turkey (TÜBİTAK 119N343).

References

[1] M.R. Krames, O.B. Shchekin, R. Mueller-Mach, G.O. Mueller, L. Zhou, G. Harbers, M.G. Craford, Status and future of high-power light-emitting diodes for solid-state lighting, J. DISP Technol. 3 (2007) 160–175.
[2] J.K. Sheu, S.J. Chang, C.H. Kuo, Y.K. Su, L.W. Wu, Y.C. Lin, W.C. Lai, J.M. Tsai, G.C. Chi, R.K. Wu, White-light emission from near UV InGaN-GaN LED chip precoated with blue/green/red phosphors, IEEE Photon. Technol. Lett. 15 (2003) 18–20.
[3] K. Li, C. Shen, White LED based on nano-YAG:Ce^{3+}/YAG:Ce^{3+},Gd^{3+} hybrid phosphors, Optik 123 (2012) 621–623.
[4] B. Chen, Q. Zhou, J. Li, F. Zhang, R. Liu, H. Zhong, B. Zou, Red emissive $CuInS_2$-based nanocrystals: a potential phosphor for warm white light-emitting diodes, Opt. Express 21 (2013) 10105–10110.
[5] C.C. Lin, R.-S. Liu, Advances in phosphors for light-emitting diodes, J. Phys. Chem. Lett. 2 (2011) 1268–1277.
[6] S. Thapa, G.C. Adhikari, H. Zhu, P. Zhu, Scalable synthesis of highly luminescent and stable thiocyanate based $CsPbX_3$ perovskite nanocrystals for efficient white light-emitting diodes, J. Alloy. Compd. 860 (2021) 158501.
[7] G.C. Adhikari, S. Thapa, Y. Yue, H. Zhu, P. Zhu, Near unity PLQY and high stability of barium thiocyanate based all-inorganic perovskites and their applications in white light-emitting diodes, Photonics Multidiscip. Digit. Publ. Inst. 8 (2021) 209.
[8] Y. Wang, H. Sun, All-inorganic metal halide perovskite nanostructures: from photophysics to light-emitting applications, Small Methods 2 (2018) 1700252.
[9] Y. Nagaoka, K. Hills-Kimball, R. Tan, R. Li, Z. Wang, O. Chen, Nanocube superlattices of cesium lead bromide perovskites and pressure-induced phase transformations at atomic and mesoscale levels, Adv. Mater. 29 (2017) 1606666.
[10] L. Protesescu, S. Yakunin, M.I. Bodnarchuk, F. Krieg, R. Caputo, C.H. Hendon, R.X. Yang, A. Walsh, M.V. Kovalenko, Nanocrystals of cesium lead halide perovskites ($CsPbX_3$, X = Cl, Br, and I): novel optoelectronic materials showing bright emission with wide color gamut, Nano Lett. 15 (2015) 3692–3696.
[11] S. Thapa, G.C. Adhikari, H. Zhu, P. Zhu, Blue-red color-tunable all-inorganic bromide–iodide mixed-halide perovskite nanocrystals using the saponification technique for white-light-emitting diodes, JOSA B 36 (2019) 1616–1622.
[12] P. Ramasamy, D.-H. Lim, B. Kim, S.-H. Lee, M.-S. Lee, J.-S. Lee, All-inorganic cesium lead halide perovskite nanocrystals for photodetector applications, Chem. Com. 52 (2016) 2067–2070.
[13] Z. Li, J. Moon, A. Gharajeh, R. Haroldson, R. Hawkins, W. Hu, A. Zakhidov, Q. Gu, Room-temperature continuous-wave operation of organometal halide perovskite lasers, ACS Nano 12 (2018) 10968–10976.
[14] H. Huang, M.I. Bodnarchuk, S.V. Kershaw, M.V. Kovalenko, A.L. Rogach, Lead halide perovskite nanocrystals in the research spotlight: stability and defect tolerance, ACS Energy Lett. 2 (2017) 2071–2083.
[15] W. Kim, J.B. Park, H. Kim, K. Kim, J. Park, S. Cho, H. Lee, Y. Pak, G.Y. Jung, Enhanced long-term stability of perovskite solar cells by passivating grain boundary with polydimethylsiloxane (PDMS), J. Mater. Chem. A 7 (2019) 20832–20839.
[16] N. Narendran, Y. Gu, J. Freyssinier-Nova, Y. Zhu, Extracting phosphor-scattered photons to improve white LED efficiency, Phys. Status Solidi A 202 (2005) R60–R62.
[17] Q. Li, K.R. Westlake, M.H. Crawford, S.R. Lee, D.D. Koleske, J.J. Figiel, K.C. Cross, S. Fathololoumi, Z. Mi, G.T. Wang, Optical performance of top-down fabricated InGaN/GaN nanorod light emitting diode arrays, Opt. Express 19 (2011) 25528–25534.

[18] Q. Jiao, Z. Chen, Y. Feng, S. Li, S. Jiang, J. Li, Y. Chen, T. Yu, X. Kang, B. Shen, The effects of nanocavity and photonic crystal in InGaN/GaN nanorod LED arrays, Nanoscale Res. Lett. 11 (2016) 1–8.
[19] V. Ramesh, A. Kikuchi, K. Kishino, M. Funato, Y. Kawakami, Strain relaxation effect by nanotexturing InGaN/GaN multiple quantum well, J. Appl. Phys. 107 (2010) 114303.
[20] L.-W. Jang, D.-W. Jeon, T. Sahoo, A.Y. Polyakov, B. Saravanakumar, Y.-T. Yu, Y.-H. Cho, J.-K. Yang, I.-H. Lee, Energy coupling processes in InGaN/GaN nanopillar light emitting diodes embedded with Ag and Ag/SiO_2 nanoparticles, J. Mater. Chem. 22 (2012) 21749–21753.
[21] A.R. Clapp, I.L. Medintz, J.M. Mauro, B.R. Fisher, M.G. Bawendi, H. Mattoussi, Fluorescence resonance energy transfer between quantum dot donors and dye-labeled protein acceptors, J. Am. Chem. Soc. 126 (2004) 301–310.
[22] C.-J. Chen, C.-C. Lin, J.-Y. Lien, S.-L. Wang, R.-K. Chiang, Preparation of quantum dot/polymer light conversion films with alleviated Förster resonance energy transfer redshift, J. Mater. Chem. C 3 (2015) 196–203.
[23] S.-H. Lee, K.-H. Lee, J.-H. Jo, B. Park, Y. Kwon, H.S. Jang, H. Yang, Remote-type, high-color gamut white light-emitting diode based on InP quantum dot color converters, Opt. Mater. Express 4 (2014) 1297–1302.
[24] H. Choi, S. Chua, A. Raman, J. Pan, A. Wee, Plasma-induced damage to n-type GaN, Appl. Phys. Lett. 77 (2000) 1795–1797.
[25] H. Park, K.H. Baik, J. Kim, F. Ren, S.J. Pearton, A facile method for highly uniform GaN-based nanorod light-emitting diodes with InGaN/GaN multi-quantum-wells, Opt. Express 21 (2013) 12908–12913.
[26] H.K. Park, S.W. Yoon, Y.J. Eo, W.W. Chung, G.Y. Yoo, J.H. Oh, K.N. Lee, W. Kim, Y.R. Do, Horizontally assembled green InGaN nanorod LEDs: scalable polarized surface emitting LEDs using electric-field assisted assembly, Sci. Rep. 6 (2016) 1–9.
[27] M. Lismont, C.A. Páez, L. Dreesen, A one-step short-time synthesis of $Ag@SiO_2$ core–shell nanoparticles, J. Colloid Interface Sci. 447 (2015) 40–49.
[28] J.-H. Yun, A.Y. Polyakov, K.-C. Kim, Y.T. Yu, D. Lee, I.-H. Lee, Enhanced luminescence of $CsPbBr_3$ perovskite nanocrystals on stretchable templates with Au/SiO_2 plasmonic nanoparticles, Opt. Lett. 43 (2018) 2352–2355.
[29] K.B. Bae, W.W. Lee, H.Y. Song, J.H. Yun, A.Y. Polyakov, I.H. Lee, Large area polymer composite films embedded with colloidal quantum dots for efficient white light generation, Phys. Status Solidi (A) 215 (2018) 1700644.
[30] D.-M. Yeh, C.-Y. Chen, Y.-C. Lu, C.-F. Huang, C. Yang, Formation of various metal nanostructures with thermal annealing to control the effective coupling energy between a surface plasmon and an InGaN/GaN quantum well, Nanotechnology 18 (2007) 265402.
[31] R. Bardhan, N.K. Grady, J.R. Cole, A. Joshi, N.J. Halas, Fluorescence enhancement by Au nanostructures: nanoshells and nanorods, ACS Nano 3 (2009) 744–752.
[32] H. Chang, Y. Hsieh, T. Chen, Y. Chen, C.-T. Liang, T.-Y. Lin, S. Tseng, L. Chen, Strong luminescence from strain relaxed InGaN/GaN nanotips for highly efficient light emitters, Opt. Express 15 (2007) 9357–9365.
[33] J.B. Schlager, K.A. Bertness, P.T. Blanchard, L.H. Robins, A. Roshko, N.A. Sanford, Steady-state and time-resolved photoluminescence from relaxed and strained GaN nanowires grown by catalyst-free molecular-beam epitaxy, J. Appl. Phys. 103 (2008) 124309.
[34] R. Bardhan, N.K. Grady, N.J. Halas, Nanoscale control of near-infrared fluorescence enhancement using Au nanoshells, Small 4 (2008) 1716–1722.
[35] W. Sigle, J. Nelayah, C.T. Koch, P.A. van Aken, Electron energy losses in Ag nanoholes—from localized surface plasmon resonances to rings of fire, Opt. Lett. 34 (2009) 2150–2152.
[36] R.F. Oulton, V.J. Sorger, T. Zentgraf, R.-M. Ma, C. Gladden, L. Dai, G. Bartal, X. Zhang, Plasmon lasers at deep subwavelength scale, Nature 461 (2009) 629–632.
[37] I.-H. Lee, L.-W. Jang, A.Y. Polyakov, Performance enhancement of GaN-based light emitting diodes by the interaction with localized surface plasmons, Nano Energy 13 (2015) 140–173.
[38] J.-H. Yun, H.-S. Cho, K.-B. Bae, S. Sudhakar, Y.S. Kang, J.-S. Lee, A.Y. Polyakov, I.-H. Lee, Enhanced optical properties of nanopillar light-emitting diodes by coupling localized surface plasmon of Ag/SiO_2 nanoparticles, Appl. Phys. Express 8 (2015) 092002.